analytical chemistry

Editors' Highlight

pubs.acs.org/ac

In Situ, Real Time Monitoring of Surface Transformation: Ellipsometric Microscopy Imaging of Electrografting at Microstructured Gold Surfaces

Sorin Munteanu,[†] Nicolas Garraud,[‡] Jean Paul Roger,[‡] Fabien Amiot,[§] Jian Shi,[⊥] Yong Chen,[⊥] Catherine Combellas,[†] and Frédéric Kanoufi*[,†]

[†]CNRS UMR 7195, ESPCI ParisTech, 10 rue Vauquelin, 75231 Paris Cedex 05, France

[‡]Institut Langevin, CNRS UMR 7587, ESPCI ParisTech, 1 rue Jussieu, 75238 Paris Cedex 05, France

[§]FEMTO-ST Institute, CNRS-UMR 6174/UFC/ENSMM/UTBM, 24 chemin de l'Épitaphe, 25030 Besançon, France

[⊥]CNRS UMR Pasteur 8640, Ecole Normale Supérieure, 24 rue Lhomond, 75231 Paris Cedex 05, France

Supporting Information

ABSTRACT: Surface chemical reactivity is imaged by combining electrochemical activation of a surface transformation process with spatiotemporal ellipsometric microscopy. An imaging ellipsometric microscope is built, allowing ellipsometric images of surfaces with a lateral resolution of ~1 μm and a thickness sensitivity of ~0.1 nm in air and 0.4 nm in a liquid. These performances are particularly adapted for using such optical setup as an in situ, real time chemical microscope to observe a chemical surface transformation. This microscope is tested for the monitoring of the electrochemically actuated diazonium grafting of a gold surface. Such reaction is a model system of organic material deposition on a gold surface induced by an electrochemical actuation. Using either plain or physically or chemically structured electrodes, it allows for the characterization of local phenomena associated with the electrografting process. This illustrates its potential to reveal the local (electro)chemical reactivity of surfaces.

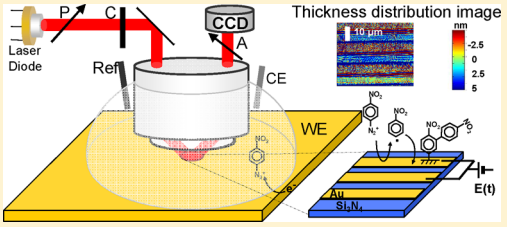

The local measurement of chemical information at a surface is of paramount importance in a wide range of applications going from the preparation and characterization of responsive surfaces to the screening of catalyst materials for energy conversion.[1] The in situ inspection of chemically microstructured surfaces can be operated using two strategies, among which includes scanning microscopies. Indeed, real time, in situ, and local chemical information is gathered with (sub)micrometric resolution by the scanning electrochemical microscope.[2] The imaging of local reaction rates is then deduced from a local electrochemical probe, a microelectrode, scanned above a surface to gather or generate local molecular fluxes.[3−5] Reactivity images are obtained from these local electrochemical currents.

Alternatively, full field optical microscopic imaging techniques allow the instantaneous imaging of a surface which, when chemically actuated, collects local chemical information. The combination of optical detection methods with electrochemical surface activation has been widely used since the early 70s for mechanistic investigations of electrochemical surface transformation. The most popular techniques are ellipsometry and, more recently, surface plasmon resonance (SPR) as both techniques are extremely sensitive to refractive index changes associated to the binding of molecular moieties on a surface. Moreover, the optical detection may be operated in an imaging microscopic mode to allow the study of local surface chemical transformations. Henceforth, electrochemical microscopes are proposed, on the basis of the combination of local optical detection associated to electrochemically activated mass or charge transfer at a surface.[6−8] However, even though highly sensitive, SPR imaging is mainly dedicated to gold surfaces deposited on transparent substrates for rear-illumination and detection. More versatile techniques are required for more general purpose analytical microsystems, such as microelectromechanical systems (MEMS).

Owing to the large popularity of ellipsometry in silicon-based microelectronic and surface science, here, we have focused on ellipsometry. Different imaging systems have been proposed or are commercially available to obtain ellipsometric images of surfaces with high spatial resolution. Originally, scanning microellipsometry was achieved by scanning a microbeam on a surface, but intrinsically, it cannot offer <10 μm spatial resolution.[9] More popular approaches use conventional ellipsometers in which a magnification (by a lens or a microscope objective) has been implemented in the analyzer arm.[10−16] However, owing to the oblique incidence, the numerical aperture of the objective that can be used without collision with the surface is limited. It also implies that the imaging device be tilted relative to the analyzed surface, which

Received: November 23, 2012
Accepted: January 27, 2013
Published: January 28, 2013

   dx.doi.org/10.1021/ac3034085 | *Anal. Chem.* 2013, 85, 1965−1971

leads to out of focus regions in the captured image. Large field inspection then requires recording a series of images that must be treated for reconstructing the ellipsometric image. Therefore, both spatial resolution and image acquisition frequency are limited, and the lateral resolution is >3 μm. Despite these drawbacks, this microscopic ellipsometry strategy is commercially available, and sensitive label-free detection modes are used in biosensors[17] and already implemented in a microfluidic environment.[18−20] It may be coupled to other techniques such as SPR imaging[21] or, more recently, to electrochemistry for the investigation of electrode surface processes.[22]

As for SPR imaging microscopy,[8] higher resolution is obtained by using a unique microscope objective for surface illumination and observation.[23−28] On the basis of this strategy, Neumaier et al. designed the imaging ellipsometric microscope, which offers the highest lateral (<1 μm) and thickness (~1 nm) resolution.[26] This setup combines the advantages of light microscopy with those of ellipsometry for the inspection of different microstructured surfaces at the air/solid or air/liquid interfaces.[27,28] It was used in our group to investigate, from ex situ observation, the local reactivity of surfaces submitted to local scanning electrochemical microscopy (SECM) patterning.[29,30]

Implemented for in situ observation, such imaging ellipsometric microscopes should provide a chemical microscope platform able to identify local reaction rates when coupled with an (electro)chemical actuation of a surface. This issue is addressed here with an optical ellipsometric setup working in the PCSA (polarizer, compensator or retarder, specimen, and analyzer) configuration.

First, the optical setup is described, and its performances are qualified. It is then used for the real time, in situ monitoring of the growth on gold electrode surfaces of nanometer thick aryl layers obtained via diazonium salts electrografting. The latter synthetic route is widely used for the decoration of various interfaces with dedicated chemical functionalities.[31] Among the mechanistic information on this chemical system, important ones relative to the film growth kinetics were already obtained by coupling electrochemical techniques to other independent in situ analytical techniques such as quartz crystal microbalance[32,33] or more recently SPR.[34] Here, we demonstrate the potentiality of imaging ellipsometric microscopy to monitor the growth of aryl layers at both global and local (micrometric) scales. The microscopic observation is particularly illustrated at electrodes micropatterned or microfabricated using standard silicon-based strategies.

PRINCIPLE OF ELLIPSOMETRIC MICROSCOPIC IMAGING

Description of the Imaging Setup and Image Processing. Ellipsometry is based on the analysis of the change of polarization of a light beam upon reflection from a surface. This polarization change is illustrated by the ratio of the complex reflection coefficients of light linearly polarized parallel (p) and perpendicular (s) to the plane of incidence, respectively r_p and r_s. The parameters measured in ellipsometry are the amplitude, tan ψ, and phase, Δ, of the ratio of these complex reflection coefficients:

$$\rho = \frac{r_p}{r_s} = \tan \Psi e^{i\Delta} \quad (1)$$

For reflection from a film-covered surface, the reflection coefficient for a given light polarization, r, is a function of the optical constants of the three involved media (ambient, film, substrate), the film thickness, and the incidence angle. Ψ and Δ are computed using eq 1 as detailed in the Supporting Information.

Here, we have built an imaging ellipsometric setup, based on the Neumaier et al.[26] configuration. It is schematized in Figure 1 and detailed in the Supporting Information (Figure S1).

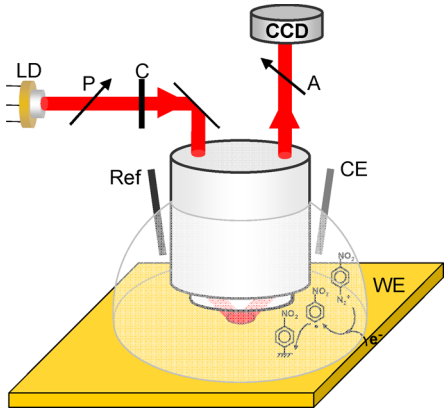

Figure 1. Schematic principle of the in situ, real time imaging of Au electrode electrografting by diazonium salt reduction owing to an ellipsometric microscope operating in the PCSA configuration. A laser light beam (from laser diode LD) polarizes (through P and C) and illuminates the Au substrate under oblique incidence obtained by a microscope objective. The observation is made in air or in liquid. The change in polarization of the reflected light is obtained by light intensity collection on the CCD camera after crossing an analyzer (A). Ref, CE, and WE are, respectively, the reference, counter, and working electrodes.

Actually, similar optical setups were shown to give confident relative variation of Ψ and Δ but not true absolute values.[27] In the framework of the optical model under scrutiny here, that is devoted to the growth of thin transparent organic layers on a substrate, Δ is the most sensitive parameter and typically presents a 1 order of magnitude higher sensitivity than Ψ. We will then more particularly seek quantitative information from relative variations of Δ. As explained in Supporting Information SI.1.4b, ellipsometric images of the spatial distribution of Δ are obtained by post-treatment of four reflected light intensity images captured on the CCD with four phase shifts of the variable retarder. An infinity-corrected high-numerical aperture microscope objective is used. To achieve angles of incidence as large as possible to provide high sensitivity, the axis of the light source beam, provided by a laser diode (637 nm), is off-centered from the optic axis of the objective: maximum angles of incidence of 54° in air and 45° in a liquid, with a beam divergence of ±~2.5°, are obtained. To perform in situ surface transformation imaging, the sample surface is illuminated from the top through an immersion microscope objective, the beam passing through the electrolytic solution.

Theoretical Performances. For a gold surface covered by a transparent organic layer (average refractive index $n_F = 1.5$) in contact with an ambient liquid or air ($n_{A,liq} = 1.33$, $n_{A,air} = 1$), the theoretical variations of Δ (details in Supporting Information SI.1.5) depend periodically on the organic layer thickness, d, as presented in Figures 2 and S3, Supporting Information. However, in the early stage of thin film growth, for

dx.doi.org/10.1021/ac3034085 | Anal. Chem. 2013, 85, 1965−1971

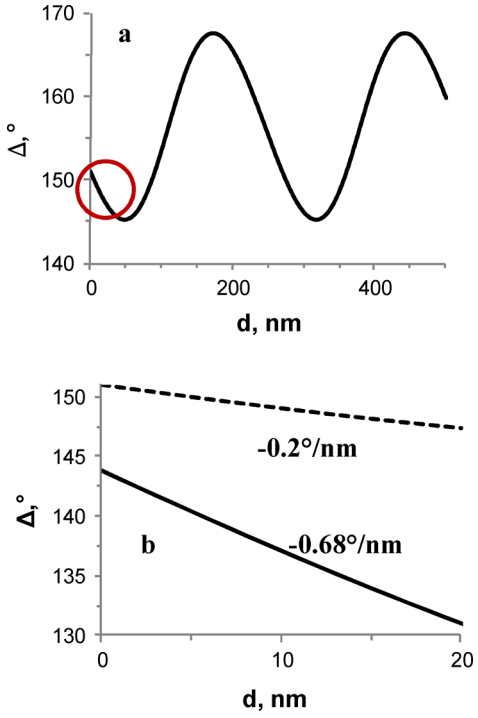

Figure 2. Theoretical evolution of the ellipsometric phase Δ as a function of the thickness of an organic film, *d*, deposited on gold. (a) Δ variation (°) for d < 500 nm in a liquid ($n_{A,liq}$ = 1.33) calculated using a one layer optical model (i.e., ambient, film, substrate) with λ = 637 nm, 45° incidence, and n_{Au} = 0.15 + 3.5i ; (b) Δ variation for d < 20 nm films in air (solid line; 55° incidence) and liquid (dashed line, red circle in a).

d < 20 nm (Figure 2b), the phase Δ decreases linearly with the film thickness, d, according to:

$$\delta\Delta = -\sigma_A d \tag{2}$$

with σ_A being the sensitivity in the given ambient medium, σ_{air} = 0.68°/nm or σ_{liq} = 0.20°/nm. In a liquid, σ is 3.4 times lower than in air, predicting a much lower sensitivity.

Experimental Performances. *Trueness and Limit of Detection.* The estimates were obtained from measurements on gold coated silicon wafers, either bare or coated with a thin organic layer obtained from the electrografting of a diazonium salt. A 5 nm thick layer, as estimated by a conventional ellipsometer, induces a variation of 3.2° in Δ when measured in air. From (2) with σ_{air} = 0.68°/nm, a calculated value of 4.7 nm is deduced. Both measurements are in close agreement, demonstrating the trueness of measurement of the ellipsometric microscope. This will be confirmed in the following by infrared spectroscopy.

The limit of detection, LOD, of the setup at each individual pixel is obtained from the standard deviation in differences of Δ obtained between two successive images, δΔ. The signal-to-noise ratio may be improved (Figure S4, Supporting Information) by accumulating a sufficient number of sets of 4 images captured to generate a resulting final image in Δ. A best compromise between acquisition time and standard deviation is obtained for 16 accumulations at a frequency of 80 Hz, which corresponds to a total duration of 2.6 s for recording one ellipsometric image, a time reasonable with film build-up from surfaces. Then, the minimal δΔ, which can be detected, is 0.08°, which corresponds to a LOD for layer thickness of 0.12 nm in air or 0.4 nm in a liquid. These performances are largely compatible with most of the deposition processes of organic or bio-organic materials on a gold surface.

Lateral Resolution. The lateral resolution was estimated through imaging of a diffraction gratings defined by periodic knife edge structures of 7 μm wide Al bands with a 3 μm interband distance (Figure S5, Supporting Information). The experimental normalized light intensity variation along the axis normal to the edge structure is fitted to the theoretical spread function given by the edge spread function, ESF:[35]

$$f_{ESF}(x) = \frac{1}{\pi} a \tan\left(\frac{x}{\alpha}\right) + \frac{1}{2} \tag{3}$$

where 2α corresponds to the lateral resolution of the imaging technique. A resolution of ∼1 μm is obtained in both air and a liquid.

RESULTS AND DISCUSSION

Ellipsometric Imaging of ex Situ Electrografted Au Surfaces. The capabilities of the ellipsometric microscope to image and quantify the chemical transformation are illustrated for Au surfaces electrografted from nitrobenzene diazonium (NBD) salt solutions. This grafting yields the anchorage of a nitrophenyl (NP) multilayer on the electrode surface. First, surfaces, which have been grafted, are observed, allowing for comparison with macroscopic ellipsometric characterization. We take advantage of the imaging capability by resolving local micrometric domains of nanometer thick organic layers within the electrodes. Figure 3a presents an image obtained in air of the δΔ distribution over a 90 × 90 μm^2 portion of a large (2 ×

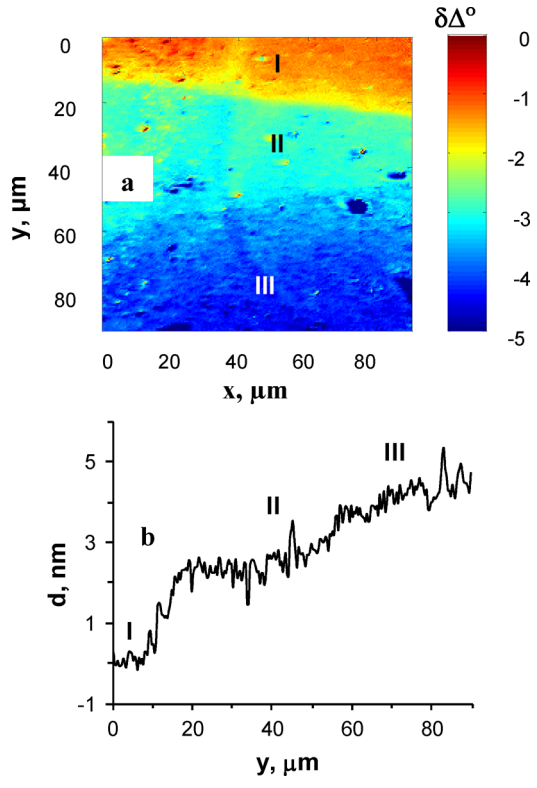

Figure 3. (a) Ellipsometric image taken in air of the transition between bare gold (I) and gold grafted (II and III) with NP film of ∼5 nm thickness; (b) evolution of the deposited thickness estimated from δΔ along a profile in the "*y*" direction.

dx.doi.org/10.1021/ac3034085 | *Anal. Chem.* 2013, 85, 1965−1971

0.5 cm^2) gold surface, half of which was electrografted ex situ with a thin NP multilayer.

As shown in Figure 3a, the grafting extent can be obtained from imaging the triple contact line (TCL) region as the latter delimitates the three media (Au, electrolytic solution, and air). Converting $\delta\Delta$ in film thickness with (2) allows one to transform the $\delta\Delta$ distribution image into a thickness distribution image, or similarly, as plotted in Figure 3b, as a profile of the thickness variation along a line in the y-axis direction. Owing to the vertical holding and incomplete immersion of the substrate in the NBD solution during the electrografting, the image presents different regions of surface coverage: the top, I, with the lowest $|\delta\Delta|$ corresponds to bare gold and the bottom, III, with the highest $|\delta\Delta|$ to the region grafted with a 5 nm thick organic layer. The middle region, II, with intermediate $\delta\Delta$ values corresponds to a 20−40 μm wide region grafted with a thinner layer. It results from the grafting at the NBD solution meniscus formed by capillarity. The structure of an electrografted film border is revealed along the TCL. The frontiers between the different regions could be fitted, in a phenomenological approach, by ESF functions (3), yielding apparent sharpness of 2.1 and 26 μm, respectively, for the frontier from I to II and II to III. The frontier between I and II corresponds to the initial position of the TCL defined by the solution meniscus. Its 2.1 μm sharpness is higher than the setup lateral resolution and indicates that the electrografting process provides diffuse-edge rather than knife-edge as can be obtained by standard lithographic techniques.[36] The large border between II and III results from the evaporation of the solution during the grafting. Inspecting the individual regions reveals the defects in the grafted surface detected either as micrometric disk domains of higher thickness (higher $|\delta\Delta|$) or as micropores (lower thickness, lower $|\delta\Delta|$), that both reproduce defects from the gold subsurface. In the capillary region II, these pores reveal the bare gold substrate.

Then, the imaging capability in a liquid was inspected. The imaging of interfacial electrografted regions (Figure S6, Supporting Information) gives results similar to those in Figure 3 taken in the air.

Real Time, in Situ Monitoring of Au Electrografting. Owing to the high stability of this optical device, images are acquired with a high resolution in a reasonable time (every 2.6 s), which allows following in situ, real time the process of film deposition. Figure 4 presents the monitoring of the electrografting of NBD at a bare Au surface (2 cm^2) performed during a chronoamperometric experiment, at a constant $E = -0.6$ V vs Ag/AgCl for 300 s. The time evolution of the spatial distribution of Δ is monitored from continuous image acquisition. Figure 4a presents the variation with time of $\delta\Delta$ averaged on a 10 × 10 μm^2 region. In the range of the measured $\delta\Delta$, the proportionality (2) between $\delta\Delta$ and the film thicknesses, d, holds, giving $\delta\Delta \sim 3°$ and $d \sim 15$ nm.

This coating is confirmed from ex situ FT-IRRAS analysis of the surface at the end of the grafting (spectrum in the inset of Figure 4a) through two strong bands at ~1350 and 1530 cm^{-1} (symmetric and asymmetric stretching), characteristic of the nitrophenyl group, and by C−C ring stretching at 1600 cm^{-1}. The thickness estimated from the ellipsometric microscope operated in situ is also in agreement with that obtained from the known correlation between the IRRAS absorbance of the nitro bands at 1351 and 1526 cm^{-1} and the NP layer thickness.[37]

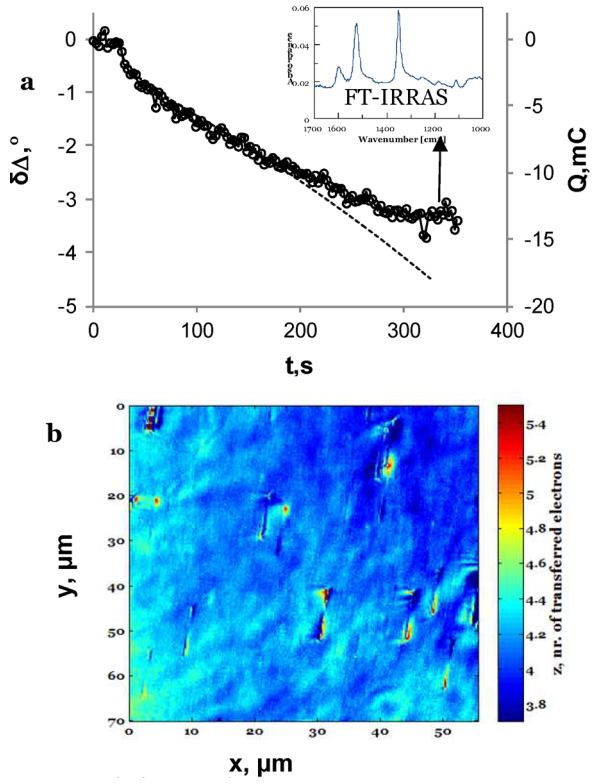

Figure 4. Real time and in situ ellipsometric monitoring of NBD electrografting on Au surface. (a) Variation of $\delta\Delta$, averaged on a 10 × 10 μm^2 (open circles) correlated with the transferred charge (dashed line), for a chronoamperometric potential step between 0.2 and −0.6 V vs Ag/AgCl for 300 s and started at t = 30 s; inset: FT-IRRAS spectrum recorded ex situ on the final grafted surface. (b) Distribution of z, the number of transferred electrons per NBD molecule during electrografting.

Furthermore, the instantaneous local thickness, estimated as in Figure 4a, is then shown to correlate nicely, at least up to 225 s, with the instantaneous charge, Q, transferred on the whole electrode during the electrografting process. It suggests that the surface coating is occurring by the same charge transfer process during the whole electrografting experiment. At longer times, the deviation indicates the decrease of the grafting efficiency as the layer is likely too thick to ensure sufficient trapping of radical species by the film. From the proportionality of Q and d, mass conservation, and Faraday's law, one obtains z, the number of electrons transferred per diazonium ion for one grafted aryl radical:

$$z = \frac{Q}{d}\frac{M}{F\rho A} \qquad (4)$$

where M = 122 g/mol is the molecular mass of the grafted aryl radical, ρ is the density of the aryl layer taken as 1 g/cm^3,[3,32] F is the Faraday constant, and A the area of the grafted electrode.

Since the generation of one radical at the electrode surface proceeds along a 1-electron process from the diazonium, z is also the number of diazonium ions that have been reduced to allow for the coupling of one radical at the electrode surface. It then gives access to the efficiency of the grafting of electrogenerated radicals, $\eta = 1/z$. From (4), the $\delta\Delta$ distribution along the surface is converted into an image of the z distribution, as depicted in Figure 4b, which indicates the local efficiency of the electrografting reaction. As in electro-

dx.doi.org/10.1021/ac3034085 | Anal. Chem. 2013, 85, 1965−1971

chemical-SPR microscopy, such electrochemical-ellipsometric image correlates local surface information (deposited thickness) to a global variable (charge transferred over the whole electrode). On the individual image obtained at the end of the grafting presented in Figure 4b, z is mainly homogeneous and varies between 4.2 and 4.4 electrons transferred per NBD moiety.

From the succession of images, the local evolution of the grafting process can be monitored and similar homogeneity is observed. It suggests that the electrografting mainly proceeds at the same rate on the whole sample surface. Systematic higher z values are observed on the right part of the image, with darker regions (dark blue), which actually correspond to uncorrected lower $\delta\Delta$ variation. A small tilt in $\delta\Delta$ is observed on all images acquired in a liquid and is actually due to residual aberrations of the imaging configuration. Despite the good overall homogeneity of the grafting, the ellipsometric image also reveals the local heterogeneity of the grafting. Indeed, small domains of 1−5 μm^2 and of higher z are regions of the surface which present lower grafting efficiency or lower coating thickness. The heterogeneity of diazonium-grafted layers and the existence of micrometric defects has already been pointed out by indirect redox probe experiments[38] or ex situ AFM images.[39] Here, these micrometric defects cover <2% of the electrode surface.

Real Time, in Situ Monitoring of Electrografting on Textured Surfaces. Ellipsometric microscopy allows one to demonstrate that the electrografting of a diazonium salt on an electrode surface is heterogeneous, revealing the regions of the electrode with different reactivity rates. In a next step, diazonium electrografting and microscopic ellipsometric imaging are combined to reveal the reactivity of textured surfaces.

Electrografting at Microbands Arrays. The ellipsometric microscope was used to monitor the electrografting at an array of Au microbands microfabricated on Si_3N_4 coated Si surfaces (8 μm wide Au bands spaced by 8 μm Si_3N_4 interbands). Figure 5a presents the Δ distribution at the array before grafting. The blue regions correspond to the Au microbands, and the red ones correspond to the Si_3N_4 substrate. Only bands 2 and 3 are electrically connected and actuated during three potential cycles (cyclic voltammetry) to generate NBD grafting. The ellipsometric image obtained at the end of the grafting is compared to the initial image. The distribution of $\delta\Delta$ in Figure 5b suggests that the connected microbands have preferentially been grafted. These darker regions are characterized by a 0.6° decrease in Δ, corresponding to a 3 nm thick grafted layer. The time evolution of the grafting was also monitored on connected and unconnected microbands during the cyclic voltammetry (Figure 5c). A thin organic layer is deposited on the connected microbands (blue trace in Figure 5c). Moreover, the coating is only effective when the electrode potential is cathodic (E < −0.4 V vs Ag/AgCl), in agreement with the need for potential activation for diazonium electrografting. The slight thickness increase observed on the unconnected bands (~0.6 nm in the red trace of Figure 5c) characterizes the extent of the spontaneous chemical grafting of a monolayer within ~300 s, in agreement with reported kinetic spontaneous growth.[37]

The characterization at such microfabricated surfaces would have been impossible with other concurrent microscopic imaging techniques and particularly with SPR imaging as the microelectrode array was deposited on a silicon wafer surface. Ellipsometric microscopy is indeed convenient to detect molecular adsorption on any microfabricated or micro-

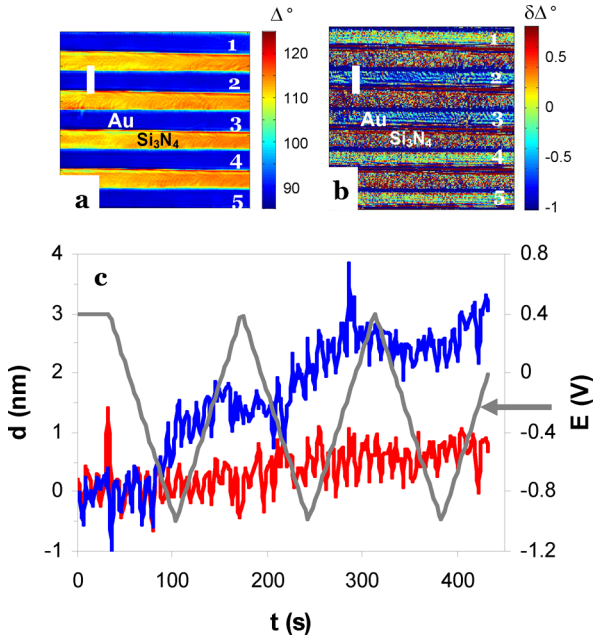

Figure 5. Real time, in situ ellipsometric imaging of NBD electrografting on Au microband arrays. (a) Δ distribution before grafting (blue: Au; yellow: Si_3N_4); (b) $\delta\Delta$ distribution at the end of the grafting when Au microbands 2 and 3 are selectively connected; scale bars, 10 μm. (c) Variation of the deposited thickness with time on 2 × 5 μm^2 zones on (blue) connected or (red) unconnected Au microbands during cyclic voltammetry (gray).

electromechanical system (MEMS), such as microcantilevers platforms. Moreover, as gold surfaces, Si-based surfaces can be characterized by ellipsometry with a high sensitivity. Unlike SPR-based microscopy, ellipsometric microscopy is able, in principle, to inspect chemical transformation processes occurring on the Si-based regions (here, the Si_3N_4 interbands regions of the array).

Such potential is detailed in Supporting Information SI.2.2 and illustrated in Figure S7, which shows the ex situ characterization of bands electrografted under highly reductive fluxes (E= −1.2 V vs Ag/AgCl). The organic coatings deposited on Au biased microbands are highly heterogeneous but reveal clearly the formation of multilayers (>150 nm). It confirms the formation of thick multilayers from catalytical growth, mediated by electrogenerating the anion radical of nitrobenzene, as already observed during the growth of thick μm layers from diazonium bearing electroactive moieties (anthraquinone, NP).[40,41]

The inspection of $\delta\Delta$ on the Si_3N_4 structures in Figure S7, Supporting Information, is also mechanistically instructive. Apart from the possible confirmation of the Si_3N_4 thickness from the difference of the ellipsometric signal between the Au and Si_3N_4 bands, the ellipsometric values Δ_{SiN} detected on interband regions adjoining grafted Au bands are systematically higher than on interband regions adjoining ungrafted Au bands. It suggests that an organic layer has been deposited in the former regions, which means that the aryl radical source can travel over a few μm. It is not consistent with the phenyl radical lifetime (~μs) unless a source of NP radicals other than the biased microbands is pointed out. As proposed for the catalytic growth of thick multilayers, the anion radical of nitrobenzene is likely this source. Indeed, this reductive species is highly stable and able to travel from its source (biased microbands) to

dx.doi.org/10.1021/ac3034085 | Anal. Chem. 2013, 85, 1965−1971

reduce NBD and generate NP radicals in the solution surrounding the microbands. Moreover, the possible diffusion of these anion radicals over μm regions is confirmed from the lateral expansion of the grafting on insulating surfaces adjoining two connected microbands. Finally, the grafting does not stand distances >5 μm in agreement with the efficient trapping of the anion radical by NBD. The electron transfer between these moieties acts as a chemical lens[30,42] that focuses the radical generation and grafting process in the vicinity of microbands sources.

Electrografting at Chemically-Patterned Surfaces. Here, the grafting of NBD is examined on a gold surface patterned by microlithography with a self-assembled monolayer. The surface was (i) modified by self-assembling of a thiol, (ii) patterned by conventional UV−vis photolithography associated to reactive ion etching (RIE) (details in Supporting Information SI.1.3), using a mask consisting of 6 μm diameter holes spaced by 15 μm, and (iii) submitted to NBD electrografting.

Figure 6a presents the ellipsometric image in a liquid (ACN) of $\delta\Delta$ distribution for the thiol-patterned Au surface. The patterns formed on the Au surface during the photolithographic procedure are characterized as holes, of negative $\delta\Delta$ values. The shape of the holes is not perfectly circular, resulting from either some heterogeneous resin transformation during the UV irradiation or heterogeneous RIE etching. Moreover, the $\delta\Delta$ difference between the regions inside and outside the holes is as high as ∼−2°, as if an organic layer of 10 nm higher thickness was present inside the patterns.

If the photolithographic procedure is assumed to locally desorb the thiol within the patterns, an ∼1 nm thickness decrease (∼0.2° $\delta\Delta$ increase) is expected within the patterns.

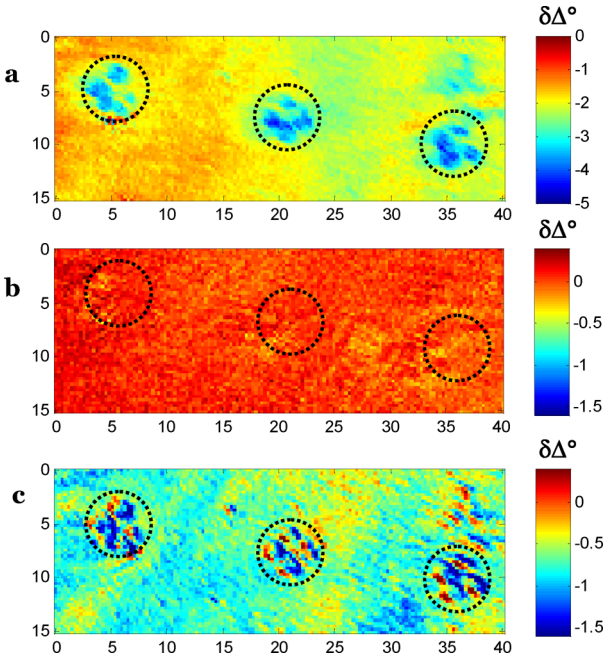

Figure 6. Ellipsometric monitoring of the electrografting of NBD on a thiol covered Au surface patterned by UV−vis lithography (disks are etched regions). (a) $\delta\Delta$ distribution evaluated in liquid, showing the patterns as regions of lower $\delta\Delta$. (b, c) $\delta\Delta$ distribution during the electrografting at the initiation (b, t = 30 s) and end (c, t = 330 s) of the electrografting; $\delta\Delta$ is evaluated by pixel by pixel comparison with the first image (a, t = 0).

The opposite and higher than expected difference in $\delta\Delta$ suggests that the RIE process has also modified the optical and chemical properties of the Au surface structure. Since RIE is performed in the presence of oxygen and highly reactive gaseous species, gold oxides are likely formed during the RIE process. Such gold oxide would act as a thin opaque layer[43] that results in lower values of Δ than for Au. The observed $\delta\Delta$, ∼−2°, is interpreted as the deposition of a gold oxide layer of ∼1 nm thickness, as estimated from optical indexes.[43] Figure 6a also shows that, if $\delta\Delta$ detected within the pattern is due to gold oxide formation, this oxide layer is not homogeneous. It is then anticipated that the patterns reactivity toward diazonium electrografting is different from that on the bare surface. The ellipsometric microscope is then a dedicated tool to inspect this local surface reactivity.

The electrografting of the patterned surface by NBD is then monitored in situ and in real time. Figure 6b presents the $\delta\Delta$ distribution measured between the images recorded at the initiation (t = 30 s) and before (t = 0) NBD electrografting. This way of data analysis actually allows one to "erase" pixel-by-pixel the heterogeneity of the initial optical response detected within the patterned surface (compare Figure 6a,b). Then, heterogeneity in local surface coating can be revealed during the grafting. This is illustrated in Figure 6c that presents the $\delta\Delta$ distribution measured between the images recorded at the end (t = 330 s) and before (t = 0) NBD electrografting. First, Figure 6c shows that the grafting operates on the whole surface, whether it is covered or not by a thiol layer. It also clearly reveals the heterogeneous nature of the electrografting process and its correlation with the lithographic patterning.

The regions where a thicker NP layer was deposited (more negative $\delta\Delta$ values) are identified in Figure 6c as those where the thiol had been etched (holes). In these regions where gold was supposed to be recovered, the surface is likely more reactive toward the anchoring of aryl radicals. The transformation of the $\delta\Delta$ image into distribution of thickness of the deposited layer indicates that ∼6 nm of a NP layer is grafted within the holes (regions within black circles), while ∼4.5 nm is grafted outside these holes. Moreover, within the holes, the region of higher deposition rates reproduces the darkest regions of the etched surface in Figure 6a and is associated to the presence of gold oxides. It suggests that the grafting of aryl radicals is likely more efficient on gold oxide surfaces.

It may also be striking that, on the thiol covered Au surface, outside the etched holes, some NP coating is observed. This can be explained either by attachment of the radical directly to the adsorbed thiol or by (partial) desorption of the thiol layer with simultaneous NP grafting. The possible potential-assisted thiol desorption step could explain the lower apparent efficiency of the grafting in the thiol covered domains.

■ CONCLUSIONS

The imaging performances of a new configuration of chemical microscope based on local ellipsometry detection are determined for the ex situ characterization, in air and in a liquid, of the deposition of nanometer thick organic layers onto a gold surface. The lateral resolution is ∼1 μm, and the thickness resolution is ∼0.1 nm in air and 0.4 nm in a liquid. These performances are adapted to use such optical setup as a chemical microscope to observe in situ and in real time a chemical surface transformation.

Since electrochemistry is a particularly appealing method to actuate a surface transformation process, we have tested this

dx.doi.org/10.1021/ac3034085 | *Anal. Chem.* 2013, 85, 1965−1971

setup during the electrochemically actuated growth of thin organic layers on gold surfaces. The ellipsometric microscope allowed one to (i) monitor quantitatively the real time, in situ electrografting of different gold surfaces by a diazonium salt, (ii) characterize local heterogeneities developed during the deposition process, and (iii) follow the heterogeneity of the electrografting process on microfabricated and patterned surfaces. This illustrates the potential of this opto-electrochemical setup to reveal the local chemical and electrochemical reactivities of surfaces. The characterization of molecular deposition at surfaces microfabricated from Si wafers would have been impossible with other concurrent label-free microscopic imaging techniques and particularly with SPR imaging. Moreover, the silicon-based surfaces can be efficiently characterized by ellipsometry with a high sensitivity. It is expected that microscopic ellipsometric imaging is a valuable tool for the label-free detection of (bio)molecular adsorption at any microfabricated or microtextured sensing platform.

■ ASSOCIATED CONTENT

Supporting Information

Experimental procedures and details. This material is available free of charge via the Internet at http://pubs.acs.org.

■ AUTHOR INFORMATION

Corresponding Author

*E-mail: frederic.kanoufi@espci.fr.

Notes

The authors declare no competing financial interest.

■ ACKNOWLEDGMENTS

Dr Y. Fedala is acknowledged for her assistance in data acquisition, C. Flammier for microfabrication of the microband array, and G. Hallais for UV−vis lithography. The "Agence Nationale de la Recherche", ANR, is gratefully acknowledged for its financial support via the ANR-08-JCJC-0088 μECOLIERS project.

■ REFERENCES

(1) Bard, A. J. *J. Am. Chem. Soc.* **2010**, *132*, 7559−7567.
(2) Wittstock, G.; Burchardt, M.; Pust, S. E.; Shen, Y.; Zhao, C. *Angew. Chem., Int. Ed.* **2007**, *46*, 1584−1617.
(3) Rodríguez-López, J.; Alpuche-Avilés, M. A.; Bard, A. J. *J. Am. Chem. Soc.* **2008**, *130*, 16985−16995.
(4) Lesch, A.; Vaske, B.; Meiners, F.; Momotenko, D.; Cortés-Salazar, F.; Girault, H. H.; Wittstock, G. *Angew. Chem., Int. Ed.* **2012**, *51*, 10413−10416.
(5) Patten, H. V.; Meadows, K. E.; Hutton, L. A.; Iacobini, J. G.; Battistel, D.; McKelvey, K.; Colburn, A. W.; Newton, M. E.; Macpherson, J. V.; Unwin, P. R. *Angew. Chem., Int. Ed.* **2012**, *51*, 7002−7006.
(6) Li, Q. G.; White, H. S. *Anal. Chem.* **1995**, *67*, 561−569.
(7) Andersson, O.; Ulrich, C.; Bjorefors, F.; Liedberg, B. *Sens. Actuators, B: Chem.* **2008**, *134*, 545−550.
(8) Shan, X.; Patel, U.; Wang, S.; Iglesias, R.; Tao, N. *Science* **2010**, *327*, 1363−1366.
(9) Erman, M.; Theeten, J. B. *J. Appl. Phys.* **1986**, *60*, 859−873.
(10) Beaglehole, D. *Rev. Sci. Instrum.* **1988**, *59*, 2557−2559.
(11) Jin, G.; Jansson, R.; Arwin, H. *Rev. Sci. Instrum.* **1996**, *67*, 2930−2936.
(12) Pak, H. K.; Law, B. M. *Rev. Sci. Instrum.* **1995**, *66*, 4972−4976.
(13) Albersdörfer, A.; Elender, G.; Mathe, G.; Neumaier, K. R.; Paduschek, P.; Sackmann, E. *Appl. Phys. Lett.* **1998**, *72*, 2930−2932.
(14) Cohn, R. F.; Wagner, J. W.; Kruger, J. *Appl. Opt.* **1988**, *27*, 4664−4671.
(15) Hénon, S.; Meunier, J. *Rev. Sci. Instrum.* **1990**, *62*, 936−939.
(16) Asinovski, L.; Beaglehole, D.; Clarkson, M. T. *Phys. Status Solidi A: Appl. Mat.* **2008**, *205*, 764−771.
(17) Bae, Y. M.; Oh, B.-K.; Lee, W.; Lee, W. H.; Choi, J.-W. *Anal. Chem.* **2004**, *76*, 1799−1803.
(18) Wang, Z. H.; Jin, G. *Anal. Chem.* **2003**, *75*, 6119−6123.
(19) Jin, G.; Meng, Y. H.; Liu, L.; Niu, Y.; Chen, S.; Cai, Q.; Jiang, T. J. *Thin Solid Films* **2011**, *519*, 2750−2757.
(20) Ross, A. M.; Zhang, D.; Deng, X.; Chang, S. L.; Lahan, J. *Anal. Chem.* **2011**, *83*, 874−880.
(21) Li, Y.-J.; Zhang, Y.; Zhou, F. *Anal. Chem.* **2008**, *80*, 891−897.
(22) Yu, Y.; Jin, G. *J. Colloid Interface Sci.* **2005**, *283*, 477−481.
(23) Rosencwaig, A.; Opsal, J.; Willenborg, D. L.; Kelso, S. M.; Fanton, J. T. *Appl. Phys. Lett.* **1992**, *60*, 1301−1303.
(24) See, C. W.; Somekh, M. G.; Holmes, R. D. *Appl. Opt.* **1996**, *35*, 6663−6668.
(25) Zhan, Q.; Leger, J. *Appl. Opt.* **2002**, *41*, 4630−4637.
(26) Neumaier, K. R.; Elender, G.; Sackmann, E.; Merkel, R. *Europhys. Lett.* **2000**, *49*, 14−19.
(27) Linke, F.; Merkel, R. *Rev. Sci. Instrum.* **2005**, *76*, 063701-1−063701-10.
(28) Linke, F.; Merkel, R. *New J. Phys.* **2005**, *7*, 128−144.
(29) Slim, C.; Tran, Y.; Chehimi, M. M.; Garraud, N.; Roger, J.-P.; Combellas, C.; Kanoufi, F. *Chem. Mater.* **2008**, *20*, 6677−6685.
(30) Nunige, S.; Hazimeh, H.; Cornut, R.; Hauquier, F.; Lefrou, C.; Combellas, C.; Kanoufi, F. *Angew. Chem., Int. Ed.* **2012**, *51*, 5208−5212.
(31) (a) Pinson, J.; Podvorica, F. I. *Chem. Soc. Rev.* **2005**, *34*, 429−439. (b) Pinson, J.; Bélanger, D. *Chem. Soc. Rev.* **2011**, *40*, 3995−4048.
(32) Laforgue, A.; Addou, T.; Bélanger, D. *Langmuir* **2005**, *21*, 6855−6865.
(33) Chernyy, S.; Bousquet, A.; Torbensen, K.; Iruthayaraj, J.; Ceccato, M.; Pedersen, S. U.; Daasbjerg, K. *Langmuir* **2012**, *28*, 9573−9582.
(34) Corgier, B. P.; Bellon, S.; Anger-Leroy, M.; Blum, L. J.; Marquette, C. A. *Langmuir* **2009**, *25*, 9619−9623.
(35) Barney Smith, E. H. *Proc. SPIE* **2006**, *6059*; Image Quality and System Performance III; doi:10.1117/12.643071.
(36) Zigah, D.; Pellissier, M.; Barrière, F.; Downard, A. J.; Hapiot, P. *Electrochem. Commun.* **2007**, *9*, 2387−2392.
(37) Busson, M.; Combellas, C.; Kanoufi, F.; Pinson, J. *Chem. Commun.* **2012**, *47*, 12631−12633.
(38) Hauquier, F.; Matrab, T.; Combellas, C.; Kanoufi, F. *Electrochim. Acta* **2009**, *54*, 5127−5136.
(39) (a) Kariuki, J. K.; McDermott, M. T. *Langmuir* **1999**, *15*, 6534−6540. (b) Noël, J.-M.; Sjoberg, B.; Marsac, R.; Zigah, D.; Bergamini, J.-F.; Wang, A.; Rigaut, S.; Hapiot, P.; Lagrost, C. *Langmuir* **2009**, *25*, 12742−12749.
(40) Bureau, C.; Levy, P.; Viel, E. PCT Int. Appl. WO 03018212, 2003.
(41) (a) Ceccato, M.; Bousquet, A.; Hinge, M.; Pedersen, S. U.; Daasbjerg, K. *Chem. Mater.* **2011**, *23*, 1551−1557. (b) Bousquet, A.; Ceccato, M.; Hinge, M.; Pedersen, S. U.; Daasbjerg, K. *Langmuir* **2012**, *28*, 1267−1275.
(42) (a) Radtke, V.; Hess, C.; Heinze, J. *Electrochim. Acta* **2009**, *55*, 416−422. (b) Hazimeh, H.; Nunige, S.; Cornut, R.; Lefrou, C.; Combellas, C.; Kanoufi, F. *Anal. Chem.* **2011**, *83*, 6106−6113.
(43) Cook, K. M.; Ferguson, G. S. *J. Phys. Chem. C* **2011**, *115*, 22976−22980.